Proton temperature anisotropy in the fast solar wind: A 16-moment bi-Maxwellian model

Xing Li
Harvard-Smithsonian Center for Astrophysics, Cambridge, Massachusetts

Abstract

A 16-moment bi-Maxwellian model to describe the proton temperature anisotropy and heat flux density in the fast solar wind is presented. Although the proton total heat flux density in this model is found to be significantly smaller than the classical Coulomb collision-dominated Spitzer-Härm heat flux density, it still plays a significant role in shaping the proton temperature anisotropy. The proton total heat flux density matches the value observed between 0.3 and 1 AU when the proton temperature is also close to the observed value. A large temperature anisotropy in the inner corona, with a proton perpendicular temperature higher than the parallel temperature, as indicated by recent ultraviolet observations, leads to a higher perpendicular heat flux. Since the perpendicular heat flux conducts energy from the perpendicular to the parallel degree of freedom, an unrealistically high parallel temperature develops in interplanetary space if no cooling mechanism for protons in the direction parallel to the magnetic field is introduced. This study suggests that with a bi-Maxwellian-based 16-moment description of the solar wind protons the high proton perpendicular temperature implied by the Ultraviolet Coronagraph Spectrometer on board Solar and Heliospheric Observatory in the inner corona and by in situ measurements from *Helios* place strong constraints on the proton heating mechanism: not only must the protons be heated in the direction perpendicular to the magnetic field, but they must also be cooled in the parallel direction.

1. Introduction

Recent observations of the profiles and intensities of the Lyman α spectral line, as well as other heavy ions, in the inner corona indicate that the random velocity distribution of protons, and other ions, in the direction perpendicular to the magnetic field is much larger than that in the parallel direction [*Kohl et al.*. 1998]. In situ measurements between 0.3 and 1 AU have also shown that the proton velocity distribution is highly anisotropic [*Marsch et al.*, 1982]. Hence the solar wind proton temperature is highly anisotropic in the inner corona and remains so in interplanetary space. In addition, the proton heat flux density measured between 0.3 and 1 AU was found to be more than 1 order of magnitude smaller than the classical Coulomb collision-dominated heat flux density [*Marsch and Richter*, 1984], most likely because of the almost collisionless nature of the solar wind plasma.

At present an empirical knowledge of the proton heat flux density from the corona out to 0.3 AU does not exist. Since the heat flux density can significantly influence the proton temperature profile, a better knowledge of the proton heat flux density is critical for the understanding of the heating and acceleration processes of the solar wind. Most solar wind models either completely ignore the proton heat flux density [*McKenzie et al.*, 1997] or simply use a modified classical heat flux density [*Hu et al.*, 1997] since the classical expression for the proton heat flux density [*Spitzer and Härm*, 1953; *Braginskii*, 1965] yields a much larger value than is observed. However, it is still not known whether the proton heat flux can be completely ignored in the inner corona and whether the proton heat flux plays a role in shaping the proton temperature anisotropy.

To explore adequately the magnitude of the proton heat flux density, transport equations including higher moments of the distribution function must be taken into account. The so-called Maxwellian-based 13-moment equations and the bi-Maxwellian-based 16-moment equations have been extensively used in studies of the polar wind [see *Blelly and Schunk*, 1993; *Demars and Schunk*, 1994, and references therein]. This general system of transport equations can be applied to both collision-dominated and collisionless flows and provides a continuous transition between the two regimes [*Schunk and Watkins*, 1979]. The solar wind flow can potentially be described by these high-moment models since Coulomb collisions may still be important in the inner corona but negligible in interplanetary space where the solar wind becomes collisionless. However, because of the numerical difficulties associated with the inclusion of higher moments, they have been practically absent in solar wind studies.

Recently, *Olsen and Leer* [1996] and *Olsen et al.* [1998] used an eight-moment approximation to model the solar wind. Ignoring the anisotropy of both electrons and protons, they found that electrons could still be regarded as a collision-dominated gas while the solar wind protons are collisionless. Because the solar wind protons show strong thermal anisotropy both in the inner corona and in interplanetary space, a complete description of the solar wind proton gas can only be achieved by a 13-moment model in which proton thermal anisotropy and total proton heat flux density are considered. In the first bi-Maxwellian-based 16-moment solar wind models developed by *Demars and Schunk* [1991], the transport equations were dramatically simplified. The 16-moment transport equations for a species: one continuity equation, three components of the momentum equation, six equations for the independent components of the symmetric pressure tensor, and six components for the parallel and perpendicular heat flow vectors that are responsible for the parallel and perpendicular energy respectively, were reduced to include only six moments in the gyrotropic limit, i.e., the density, field-aligned flow velocity, parallel and perpendicular temperatures, and field-aligned parallel and perpendicular heat flux density. *Demars and Schunk* [1991] considered the temperature anisotropies of electrons and protons together with the parallel and perpendicular heat flux densities associated with the parallel and perpendicular (to the magnetic field) energy equations. However, their models were typical of a slow solar wind, and their computations started at 28 R_S. Hence the fast solar wind and the key solar wind acceleration region, i.e., the first several solar radii, were not explored. The effect of the interplanetary spiral magnetic field was also ignored. More recently, *Olsen and Leer* [1999] presented solar wind models based on gyrotropic transport equations from the coronal base to 30 R_S, and found a strong energy transport between the parallel and perpendicular degrees of freedom in the inner corona.

In this paper a 16-moment fast solar wind model based on a bi-Maxwellian proton velocity distribution from the coronal base to 1 AU is presented. Since protons play a dominant role in the solar wind heating and acceleration processes, the 16-moment description is applied to the protons only, while the anisotropy of electrons is neglected. The effect of the interplanetary spiral magnetic field on transport processes is also included in the models.

2. Model Description

2.1. Governing Equations

The generalized transport equations for a multicomponent anisotropic plasma follow those given by *Barakat and Schunk* [1982]. In order to close the system of transport equations it is necessary to adopt an approximate expression for the distribution functions of the different species. The bi-Maxwellian-based 16-moment transport equations are derived by taking velocity moments of the Boltzmann equation, assuming that the distribution function has the following form [*Oraevskii et al.*, 1968; *Demars and Schunk*, 1990]:

$$f = f_B(1+\Theta_B), \tag{1}$$

where

$$f_B = n\left(\frac{m}{2\pi k_B T_\parallel}\right)^{1/2}\left(\frac{m}{2\pi k_B T_\perp}\right) \cdot \exp\left(-\frac{m}{2k_B T_\parallel}c_\parallel^2 - \frac{m}{2k_B T_\perp}c_\perp^2\right) \tag{2}$$

is the bi-Maxwellian distribution and Θ_B is a correction factor. The transport equations given by *Barakat and Schunk* [1982] can be greatly simplified if the stress tensor is ignored and only transport parallel to the magnetic field is considered. In this case, $q_\parallel$ and $q_\perp$, the parallel and perpendicular heat flow densities of a species, representing the field-aligned flow of parallel and perpendicular energy components, may adequately describe the heat flow of the species. The correction factor Θ_B can then be written as [*Demars and Schunk*, 1990]

$$\Theta_B = -\frac{\beta_\perp\beta_\parallel q_\perp c_\parallel}{\rho}(1-\frac{1}{2}\beta_\perp c_\perp^2) - \frac{\beta_\parallel^2 q_\parallel c_\parallel}{2\rho}(1-\frac{1}{3}\beta_\parallel c_\parallel^2). \tag{3}$$

In the above expression, $\beta_\parallel = \frac{m}{k_B T_\parallel}$, $\beta_\perp = \frac{m}{k_B T_\perp}$, $T_\parallel$ and $T_\perp$ are the parallel and perpendicular temperatures of the plasma species that are being described, $c_\parallel$ and $c_\perp$ are the components of the thermal velocity parallel and perpendicular to the magnetic field, and k_B is the Boltzmann constant. The species mass and number density are given by m and n, respectively, and $\rho = nm$ is the mass density.

For a two-fluid, electron-proton solar wind with ani-sotropic proton temperature the one-dimensional time-dependent bi-Maxwellian based 16-moment transport equations can be found in *Demars and Schunk* [1991], *Ganguli et al.* [1987], and *Ganguli and Palmadesso* [1987], where the plasma is assumed to flow along the direction of the magnetic field. These equations have been reduced to include only six moments by just considering transport parallel to the magnetic field and neglecting the stress tensor. If the effect of the interplanetary spiral magnetic field is included and the solar wind speed v is along the radial direction, the reduced transport equations can be derived from *Barakat and Schunk* [1982] as

$$\frac{\partial n}{\partial t} + \frac{1}{a}\frac{\partial}{\partial r}(nva) = 0, \tag{4}$$

$$\begin{aligned}
&\frac{\partial v}{\partial t} + v\frac{\partial v}{\partial r} + \frac{k_B}{m_p}\left(\frac{\partial T_{p\parallel}}{\partial r}\cos^2\Phi + \frac{\partial T_{p\perp}}{\partial r}\sin^2\Phi + \frac{\partial T_e}{\partial r}\right) \\
&+\frac{k_B}{nm_p}\left(T_{p\parallel}\cos^2\Phi + T_{p\perp}\sin^2\Phi + T_e\right)\frac{\partial n}{\partial r} \\
&+\frac{k_B}{am_p}\left(T_{p\parallel} - T_{p\perp}\right)\frac{\partial}{\partial r}\left(a\cos^2\Phi\right) \\
&-\frac{k_B}{m_p}\frac{1}{a}\frac{da}{dr}\left(T_{p\parallel} - T_{p\perp}\right)\sin^2\Phi + \frac{GM_s}{r^2} - \frac{D}{nm_p} = 0,
\end{aligned} \tag{5}$$

$$\begin{aligned}
&\frac{\partial T_e}{\partial t} + v\frac{\partial T_e}{\partial r} + \frac{2T_e}{3a}\frac{\partial}{\partial r}(va) + \frac{2}{3nk_B a}\frac{\partial}{\partial r}\left(q_e a\cos\Phi\right) \\
&+2\nu_{pe}\left(T_e - T_p\right) - \frac{2}{3nk_B}(Q_e - L_{\mathrm{rad}}) = 0,
\end{aligned} \tag{6}$$

$$\begin{aligned}
&\frac{\partial T_{p\parallel}}{\partial t} + v\frac{\partial T_{p\parallel}}{\partial r} + 2T_{p\parallel}\cos^2\Phi\frac{\partial v}{\partial r} + \frac{1}{a}\frac{\mathrm{d}a}{\mathrm{d}r}vT_{p\parallel}\sin^2\Phi \\
&+\frac{1}{nk_B a}\frac{\partial}{\partial r}\left(aq_{p\parallel}\cos\Phi\right) - \frac{2q_{p\perp}}{nk_B a}\frac{\partial(a\cos\Phi)}{\partial r} \\
&+2\nu_{pe}\left(T_{p\parallel} - T_e\right) + \frac{4}{5}\nu_{pp}\left(T_{p\parallel} - T_{p\perp}\right) - \frac{2}{nk_B}Q_{p\parallel} = 0,
\end{aligned} \tag{7}$$

$$\begin{aligned}
&\frac{\partial T_{p\perp}}{\partial t} + v\frac{\partial T_{p\perp}}{\partial r} + T_{p\perp}\sin^2\Phi\frac{\partial v}{\partial r} - \frac{1}{2a}\frac{\mathrm{d}a}{\mathrm{d}r}vT_{p\perp}\sin^2\Phi \\
&+\frac{1}{nk_B a}\frac{\partial}{\partial r}\left(aq_{p\perp}\cos\Phi\right) + \frac{q_{p\perp}}{nk_B a}\frac{\partial(a\cos\Phi)}{\partial r} + \frac{vT_{p\perp}}{a}\frac{\mathrm{d}a}{\mathrm{d}r} \\
&+2\nu_{pe}\left(T_{p\perp} - T_e\right) - \frac{2}{5}\nu_{pp}\left(T_{p\parallel} - T_{p\perp}\right) - \frac{1}{nk_B}Q_{p\perp} = 0.
\end{aligned} \tag{8}$$

$$\begin{aligned}
&\frac{\partial q_e}{\partial t} + v\frac{\partial q_e}{\partial r} + \frac{q_e}{5}\frac{\partial v}{\partial r}(7+9\cos^2\Phi) + \frac{vq_e}{5}\frac{\partial a}{\partial r}(7+4.5\sin^2\Phi) \\
&+\frac{5}{2}\frac{nk_B^2 T_e}{m_e}\cos\Phi\frac{\partial T_e}{\partial r} + \frac{4}{5}\nu_e' q_e = 0.
\end{aligned} \tag{9}$$

$$\frac{\partial q_{p\parallel}}{\partial t}+v\frac{\partial q_{p\parallel}}{\partial r}+(1+3\cos^2\Phi)q_{p\parallel}\frac{\partial v}{\partial r}+\frac{vq_{p\parallel}}{a}\frac{\partial a}{\partial r}(1+1.5\sin^2\Phi)$$
$$+3nT_{p\parallel}\cos\Phi\frac{k_B^2}{m_p}\frac{\partial T_{p\parallel}}{\partial r}+\frac{4}{5}\nu_{pp}q_{p\parallel}=0, \qquad (10)$$

$$\frac{\partial q_{p\perp}}{\partial t}+v\frac{\partial q_{p\perp}}{\partial r}+2q_{p\parallel}\frac{\partial v}{\partial r}+\frac{2vq_{p\parallel}}{a}\frac{\partial a}{\partial r}+nT_{p\parallel}\cos\Phi\frac{k_B^2}{m_p}\frac{\partial T_{p\perp}}{\partial r}$$
$$+\frac{1}{a}\frac{\partial(a\cos\Phi)}{\partial r}\frac{k_B^2}{m_p}nT_{p\perp}(T_{p\parallel}-T_{p\perp})+\frac{4}{5}\nu_{pp}q_{p\perp}=0. \qquad (11)$$

Neutrality and zero current are assumed so that $n_e \approx n_p = n$ and $v_e \approx v_p = v$. The electron temperature is T_e. The proton temperatures parallel and perpendicular to the magnetic field are $T_{p\parallel}$ and $T_{p\perp}$, respectively. The mean proton temperature is defined as $T_p = (T_{p\parallel} + 2T_{p\perp})/3$. The electron heat flux density is q_e, and the proton parallel and perpendicular heat flux densities (corresponding to the proton parallel and perpendicular energy equations) are $q_{p\parallel}$ and $q_{p\perp}$, respectively. The proton total heat flux density is defined as $q_p = (q_{p\parallel} + 2q_{p\perp})/2$. The collision frequencies ν_{pe} and ν_{pp} are

$$\nu_{pe}=\frac{4\sqrt{2\pi m_e}\,ne^4\ln\Lambda}{3m_pk_B^{3/2}T_e^{3/2}}\ ,\quad \nu_{pp}=\frac{4\sqrt{\pi}\,ne^4\ln\Lambda}{3\sqrt{m_p}k_B^{3/2}T_p^{3/2}}\ , \qquad (12)$$

where the Coulomb logarithm $\ln\Lambda$ is taken to be 23, and ν_e' is defined by [e.g., *Schunk and Watkins*, 1979]

$$\nu_e'=0.42\left[\nu_{ee}+\frac{13}{8}\nu_{ep}\right]\ ,\quad \nu_{ee}=\frac{4\sqrt{\pi}\,ne^4\ln\Lambda}{3\sqrt{m_e}k_B^{3/2}T_e^{3/2}}\ ,$$
$$\nu_{ep}=\sqrt{2}\nu_{ee}. \qquad (13)$$

The collisional terms used in this model are from *Burgers* [1969] for the case of Coulomb collisions [see, e.g., *Ganguli et al.*, 1987; *Gombosi and Rasmussen*, 1991]. These collisional terms are derived from an approximation to integrate the collisional term in the Boltzmann equation. As proposed by *Bhatnagar et al.* [1954], *Gross and Krook* [1956] and *Krook* [1955], the Bhatnagar-Gross-Krook approximation was originated to treat the various collisional regimes from the collision-dominated to the weakly collisional. With this approximation the collisional term in the Boltzmann equation (often referred to as BGK equation) can be integrated in a very simple way. *Livi and Marsch* [1986] found that the BGK approximation gave results for the ratio $T_\perp/T_\parallel$ that were accurate to within 25% when the initial ratio was 4. The collisional terms are different from those used by *Demars and Schunk* [1991] and *Olsen and Leer* [1999], who adopted very complicated collisional terms that were obtained from the bi-Maxwellian collision terms for Coulomb interactions presented by *Demars and Schunk* [1979].

Strictly speaking, (4)—(11) are valid only in the gyrotropic limit, namely, in the limit of an infinitely strong magnetic field [see, *Gombosi and Nagy*, 1988; *Gombosi and Rasmussen*, 1991], when the coefficients of the magnetic field should vanish in all the transport equations: the momentum, pressure tensor, and heat flux equations [*Gombosi and Nagy*, 1988]. In the outer solar wind (e.g., 1 AU) the magnetic field pressure is not strong compared to the plasma thermal pressure. However, there are several reasons why these equations can still be used. First, zero current assumption removes the Lorentz force term from the momentum equation. Second, in situ measurements have shown field-aligned velocity distributions [*Marsch et al.*, 1982]. Hence it may be reasonable to assume that there are only two independent pressure components, the parallel and perpendicular average random energy components, and to omit stress tensors, even though stress tensors are not zero in reality. Third, it is well documented that the solar wind heat flux is field-aligned [*Marsch*, 1991]. Hence it is appropriate to assume that the heat flow tensor has only two independent field-aligned components $q_\parallel$ and $q_\perp$. The second and third assumptions make it possible to ignore the coefficients of the magnetic field in the equations of pressure tensor and heat flow vectors [*Gombosi and Nagy*, 1988]. Therefore, (4)—(11) can be reliably adopted even though the spiral magnetic field is included.

The electron and proton mass is m_e and m_p, M_s and G are the mass of the Sun and the gravitational constant, respectively, and Φ is the angle between the magnetic field and the radial direction given by

$$\tan\Phi=\begin{cases}(\Omega r/v)\sin\theta & r>10R_S\\ 0 & r\le 10R_S\end{cases} \qquad (14)$$

Here $\Omega = 2.7\times10^{-6}\ \mathrm{rad\,s^{-1}}$ is the angular velocity of the Sun, and θ is the heliospheric colatitude taken to be $\pi/2$ in this study. The cross section of a flow tube is $a = r^2 f(r)$ with

$$f(r)=\frac{f_m e^{(r-r_a)/\sigma_a}+1-(f_m-1)e^{(R_S-r_a)/\sigma_a}}{e^{(r-r_a)/\sigma_a}+1} \qquad (15)$$

taken from *Kopp and Holzer* [1976]. Here f_m, r_a, and σ_a are constants, and R_S is the radius of the Sun.

Since the heating mechanism for the solar wind is presently unknown, the following ad hoc heating functions are used in our calculations [e.g., *Withbroe*, 1988]

$$
\begin{aligned}
&Q_e = Q_{e0} e^{(R_S - r)/\sigma_e}, \\
&Q_{p\perp} = Q_{p1} e^{(R_S - r)/\sigma_p} + Q_{p2}\left(1 - e^{(R_S-r)/(10R_S)}\right)\frac{R_S^4}{r^4}, \\
&Q_{p\|} = Q_{p3}\left(1 - e^{(R_S-r)/(10R_S)}\right)\frac{R_S^4}{r^4},
\end{aligned}
\tag{16}
$$

where Q_{e0}, σ_e, Q_{pi} $(i = 1, 2, 3)$, and σ_p are constants. The additional heating function $Q_{p\perp}$ consists of two parts: one corresponds to a local heating at the coronal base and the other corresponds to an extended heating similar to that used by *Hu et al.* [1997] and *McKenzie et al.* [1997]. The function L_{rad} describing the radiative energy loss in the electron energy equation is assumed to have the form parameterized by *Rosner et al.* [1978] for an optically thin medium. We also utilize a momentum addition function of the form

$$D = D_0 e^{(R_S - r)/\sigma_d}, \tag{17}$$

where D_0 and σ_d are constants.

2.2. Computational Approach

A fully implicit time-dependent one-dimensional two-fluid solar wind code is used to solve (1) — (8). Details of the computational scheme are given by *Hu et al.* [1997]. One thousand nonuniformly distributed grid points are used to cover the distance from 1 to 258 R_S. The smallest grid distance is $\sim 10^{-6} R_S$ at the coronal base, which guarantees a very good accuracy when gradients are steepest. The maximum error in any of the conserved quantities is <1% after a steady state is reached. The densities and temperatures of all species are kept fixed at the coronal base. The velocity of the protons at the coronal base is determined by the mass conservation relation, $v^1 = v^2 a^2 n^2/(a^1 n^1)$, the superscripts 1 and 2 denote the first two grid points. As for the heat flux densities, the following boundary conditions

$$q_i^1 = q_i^2 + \theta(q_i^2 - q_i^3)\ , \quad i = e\ , \quad p\,\|\ , \quad p\perp \tag{18}$$

are used at the coronal base. The superscripts 1, 2, and 3 denote the first three grid points at the coronal base. The parameter θ can be chosen in the range $0 < \theta < 1$; however, the model is not sensitive to the value of θ chosen. Linear extrapolation is used for all quantities at the outer boundary (i.e., 258 R_S).

The computational approach used here is different from that of *Demars and Schunk* [1991], where temperatures and heat flux densities were fixed either at the inner or outer boundary. In the approach used here, only the coronal base temperatures and proton heating are specified since the temperature gradients cannot be predicted and since the heat flux densities are very sensitive to the temperature gradients.

3. Computational Results

The following conditions at $r = 1R_S$ are adopted in the model calculations:

$$
\begin{aligned}
&(n_e)_{1R_S} = 2.5 \times 10^8\ \mathrm{cm}^{-3}\ , \\
&(T_e = T_{p\|} = T_{p\perp})_{1R_S} = 6 \times 10^5\ \mathrm{K}.
\end{aligned}
\tag{19}
$$

The corresponding base pressure is consistent with the values given by *Withbroe* [1977, 1988] and *Dulk et al.* [1977] in coronal holes. The main empirical constraints imposed on a fast solar wind solution are the wind velocity, temperature, and mass flux measured at 1 AU [*Marsch et al.*, 1989; *Goldstein et al.*, 1996]. Constraints in the inner corona are those inferred from remote sensing ultraviolet observations in coronal holes [*Kohl et al.*, 1998].

3.1. Models Without Heating $T_{p\|}$

We first explore fast solar wind models with no additional heating or cooling for protons in the direction parallel to the magnetic field ($Q_{p\|} = 0$). Since the divergence of field lines is unknown, two extreme examples are given: model 1 for a radial expansion and model 2 for a rapidly diverging flow tube, with the following sets of parameters:

Model 1

$$
\begin{aligned}
&f_m = 1\ , \quad \sigma_e = 0.18 R_S, \\
&Q_{e0} = 2.2 \times 10^{-6} \mathrm{erg\ cm^{-3}\ s^{-1}}, \\
&Q_{p1} = 2 \times 10^{-7} \mathrm{erg\ cm^{-3}\ s^{-1}}\ , \quad \sigma_p = 0.72 R_S\ , \\
&Q_{p2} = 1.6 \times 10^{-6} \mathrm{erg\ cm^{-3}\ s^{-1}}\ , \\
&D_0 = 3 \times 10^{-16} \mathrm{g\ cm^{-2}\ s^{-2}}\ , \quad \sigma_d = 1.8 R_S\ ,
\end{aligned}
\tag{20}
$$

Model 2

$$
\begin{aligned}
&f_m = 6\ , \ r_a = 1.31 R_S\ , \ \sigma_a = 0.51 R_S\ , \\
&Q_{e0} = 1.9 \times 10^{-6} \mathrm{erg\ cm^{-3}\ s^{-1}}\ , \ \sigma_e = 0.23 R_S\ , \\
&Q_{p1} = 1 \times 10^{-6} \mathrm{erg\ cm^{-3}\ s^{-1}}\ , \quad \sigma_p = 0.4 R_S\ , \\
&Q_{p2} = 2.2 \times 10^{-6} \mathrm{erg\ cm^{-3}\ s^{-1}}\ , \\
&D_0 = 3 \times 10^{-15} \mathrm{g\ cm^{-2}\ s^{-2}}\ , \quad \sigma_d = 0.77 R_S.
\end{aligned}
\tag{21}
$$

The solid and dashed lines in Figure 1 correspond to models 1 and 2, respectively. The wind speed, electron density, temperatures, and heat flux densities Figure 1 are displayed in Figures 1a, 1b, 1c, and 1d, respectively. The solid circles represent the observed upper and lower perpendicular temperatures of neutral hydrogen derived from the line width measurements of neutral hydrogen Lyα line in coronal holes [*Kohl et al.*, 1998], and the triangles and stars represent the perpendicular and parallel proton temperatures observed by *Helios* [*Marsch et al.*, 1982]. The two models yield mass fluxes within the range measured at 1 AU: $n_E v_E$ is 2.21 and 2.24×10^8 cm^{-2} s^{-1} in models 1 and 2, respectively. Because of the combined effect of a faster than radially expanding flow tube and a greater momentum addition, the solar wind in model 2 accelerates much faster in the inner corona than in model 1. The proton parallel temperature between 2 and 3 R_S in model 2 is lower than that in model 1 because of the faster wind acceleration there (see the term associated with $\partial v/\partial r$ in (7)). The proton perpendicular temperature in models 1 and 2 follows the observed hydrogen effective temperature from the Ultraviolet Coronagraph Spectrometer (UVCS) fairly well. The electron temperature below 1.2 R_S is close to that given by *David et al.* [1998] and *Wilhelm et al.* [1998]. *Wilhelm et al.* [1998] reported that the electron temperature is between 7.5×10^5 and 8.8×10^5 K at a similar height in an interplume lane in a coronal hole, while *David et al.* [1998] reported T_e to be $\sim 8\times10^5$ K at 1.15 R_S. Because of the almost identical extended heating in the perpendicular direction, the proton perpendicular temperature between 0.3 and 1 AU is close to the in situ observed values from *Helios*. However, the proton parallel temperature of the two models in interplanetary space is much higher than the observed value.

Because of the rapid acceleration, the cooling of the protons in the direction parallel to the magnetic field due to the radial expansion of the fast solar wind is only important in the inner corona [*Hu et al.*, 1997; *Li et al.*, 1999]. The almost collisionless nature of the wind makes the cooling terms associated with collisions negligible. *Hu et al.* [1997] demonstrated that the cooling effect of the spiral magnetic field is small too. Hence it is difficult to cool the protons in the direction parallel to the magnetic field in interplanetary space. This becomes even more difficult in the 16-moment models since the proton perpendicular heat flux density can conduct energy to or away from the parallel degree of freedom. The coupling between the parallel and perpendicular degrees of freedom is due to the flow tube expansion (see term

$$-\frac{2q_{p\perp}}{nk_Ba}\frac{\partial(a\cos\Phi)}{\partial r}$$

in (7)) as indicated by *Hollweg* [1986]. It must be pointed out that this term is often ignored in the literature [*Leer and Axford*, 1972; *Sandbæk*, 1994; *Hu et al.*, 1997; *Li et al.*, 1999]. From (7) it is readily seen that if $q_{p\perp}$ is greater than zero, $q_{p\perp}$ will heat $T_{p\|}$. In these models a higher perpendicular than parallel temperature in the inner corona leads to a greater perpendicular than parallel heat flux density (see $T_{p\|}$ between 2 and 20 R_S in Figure 1c), and the perpendicular heat flux density is positive. That is why $T_{p\|}$ increases between 2 R_S and 50 R_S (as seen in Figure 1c). This additional heating causes the proton parallel temperature to gain nonrealistically high values beyond 0.3 AU. We also see from Figures 1c and 1d that when the proton temperature reaches a maximum or minimum, the corresponding heat flux density is not zero. For the classical collision-dominated concept of the heat flux, on the other hand, the heat flux density would have been zero at the extrema. Hence this example shows that the classical description is not valid for the fast solar wind.

Shown in Figure 2 are the ratios between the electron and proton heat flux densities q_e and q_p computed from our models and the classical heat flux densities q_{ec} and q_{pc}. The classical heat flux densities are given by Figure 2

$$\begin{aligned} q_{ec} &= 8\times10^{-7}T_e^{5/2}\tfrac{dT_e}{dr}\,,\\ q_{pc} &= 3.2\times10^{-8}T_p^{5/2}\tfrac{dT_p}{dr}\,, \end{aligned} \tag{22}$$

where T_e and T_p are values derived from the computations. It is seen that the electron heat flux density is very close to its classical value. The maximum relative difference is smaller than 25%, as shown originally by *Olsen and Leer* [1996], who treated the electrons in a similar manner. The discontinuities between 1 and $2R_S$ are due to the existence of an electron temperature maximum, where the electron classical heat flux density is zero. Hence the classical Coulomb collision-dominated concept of the electron heat flux is still valid for the fast solar wind. However, we must keep in mind that the electrons observed in interplanetary space are also highly anisotropic in the fast solar wind. In that case the electron heat flux density may be different; a problem that remains to be explored.

On the other hand, the classical Coulomb collision-dominated concept of the proton heat flux completely breaks down in the models since q_p is found to be much smaller than its classical values except at the coronal base. The discontinuities in the ratio q_p/q_{pc} are caused by either a peak in the proton temperature or a zero proton total heat flux density $q_p = (q_{p\parallel} + 2q_{p\perp})/2$. The ratio q_p/q_{pc} can have negative values, implying that the collisionless proton heat flux does not necessarily conduct thermal energy from high- to low-temperature regions. In most of the computational domain the proton heat flux density is more than 2 orders of magnitude smaller than its classical value. However, the proton heat flux density is still important for shaping the proton thermal anisotropy. If the proton heat flux density is completely ignored, the proton parallel temperature will be much lower than that observed at 1 AU even though the wind parameters such as flow speed and mass flux will change only slightly at 1 AU [*Li*, 1999]. Hence the proton heat flux density plays an important role in conducting thermal energy from the Sun to interplanetary space.

Figure 3

By supplying values of the macroscopic plasma parameters one obtains two-dimensional contour plots of the proton distribution function f showing how its shape varies as a function of $c_\parallel$ and $c_\perp$. Using the parameters of model 2, we show in Figure 3 two-dimensional contour plots for protons at different heliocentric distances in the plane defined by the magnetic field vector and an arbitrary direction vector in the velocity space ($c_\parallel$ is shifted to the solar wind corotating frame). The dotted contour at $5R_S$ represents a negative value of -0.005. There is no dotted line in velocity distribution contours at other heliospheric distances, which means that the absolute value of the smallest negative value is < 0.005. The transition from the collision-dominated to the collisionless-dominated region is clearly shown in Figure 3. At the coronal base ($1R_S$) where collisions are strong the velocity distribution is almost exactly Maxwellian. At $1.4R_S$ the collisions cannot keep protons isotropic, but the velocity distribution is roughly bi-Maxwellian. The velocity distribution is already substantially skewed at $2R_S$ and dramatically so at $5R_S$ where the perpendicular heat flux $q_{p\perp}$ is very strong. After 20 R_S the distribution function becomes more bi-Maxwellian since q_p is relatively smaller than in the inner corona. Since there is no efficient mechanism to cool $T_{p\parallel}$, $T_{p\parallel}$ is much larger than $T_{p\perp}$ beyond 40 R_S in these models. The proton parallel temperature is much flatter than is observed. The distribution function beyond 100 R_S shown in Figure 3 is quite different from the observed ones.

3.2. Model With Cooling of $T_{p\parallel}$

Protons can be significantly cooled in the direction parallel to the magnetic field if an appropriate cooling mechanism is invoked [*Li et al.*, 1999]. For illustration purposes, here we simply use an ad hoc function (see (16)) to reproduce the effect of parallel cooling. The parameters in (21) are used with $Q_{p3} = -2.5\times10^{-7}$erg cm^{-3} s^{-1}. The results of model 3 are shown in Figure 4. To compare with observations, the upper and lower limit of the total ion heat flux in the fast solar wind [*Marsch and Richter*, 1984] are shown as crosses in Figure 4d. It is clear that $T_{p\parallel}$ in model 3 matches in situ measurements much better than in model 2. Since the adopted parallel cooling primarily occurs after 10 R_S, the solar wind energy balance is influenced only slightly, and the solar wind flow speed and mass flux at 1 AU are unchanged. However, the enhanced proton parallel temperature gradient increases the total proton heat flux density significantly between 0.3 and 1 AU. In model 3, q_p lies at the lower limit of the observed total ion heat flux [*Marsch and Richter*, 1984], while q_p is much smaller than the observed values between 0.3 and 1 AU in both models 1 and 2 (not shown in Figure 1). Since minor ions might be responsible for a fraction of the observed heat flux, the match between the model and observations is reasonably good considering that only protons are included in the calculations. Figure 4

For comparison, contour plots of the two-dimensional velocity distribution for model 3 are shown in Figure 5. It is readily seen that the proton velocity distribution of model 3 is quite similar to that of model 2 except that the distribution is strongly skewed beyond $10R_S$ (compare with Figure 3) because of a larger heat flux density. A typical proton velocity distribution beyond 0.3 AU has a much wider perpendicular than parallel core temperature, while protons have a high energy tail in the direction parallel to the magnetic field [*Marsch et al.*, 1982]. However, the velocity distribution contours in Figure 5 fail to produce this feature, probably because of the still lower than observed heat flux density between 0.3 and 1 AU. Because only ad hoc functions are invoked to heat or cool the solar wind in the present model, the resulting proton temperature profiles between 0.3 and 1 AU are flatter than observed. *Demars and Schunk* [1990] have shown that the double-hump proton velocity distribution can be achieved by allowing the total heat flux to be 50% larger than the observed Figure 5 value, which is probably within the experimental uncertainty, and by assuming a ratio $q_{p\|}/q_{p\perp}$ as large as 10. The produced velocity distribution function will have significant negative values in some velocity space. *Leblanc and Hubert* [1997] concluded that the 16-moment bi-Maxwellian approximation cannot generate the double-humped profiles. We notice that negative values occur in some velocity space (see the dotted contours) at $5R_S$ and $10R_S$, even though they are only slightly smaller than 0. We will return to this issue later in section 3.4.

3.3. Model Without Momentum Addition and Extended Heating

In models 1, 2, and 3, extended heating (Q_{p2} and Q_{p3} in (16)) and momentum addition (D_0 in (17)) were applied to protons in order to match observations. The momentum addition given to protons can lead to a considerable parallel cooling in the inner corona as shown by *Olsen and Leer* [1999]. The extended heating and cooling significantly decrease the difference between $T_{p\|}$ and $T_{p\perp}$ in the outer solar wind.

Figure 6

Shown in Figure 6 is a model with $Q_{p2} = Q_{p3} = D_0 = 0$ and with the following parameters:

Model 4

$$
\begin{aligned}
&f_m = 1\ , \quad \sigma_e = 0.25R_S, \\
&Q_{e0} = 4. \times 10^{-7}\text{erg cm}^{-3}\ \text{s}^{-1}\ , \\
&Q_{p1} = 5 \times 10^{-7}\text{erg cm}^{-3}\ \text{s}^{-1}\ , \quad \sigma_p = 0.72R_S.
\end{aligned} \tag{23}
$$

This model yields a solar wind speed of 615 km s^{-1} and a mass flux of 2.05 $\times 10^8$ cm^{-2} s^{-1} at 1 AU. It is readily seen in Figure 6 that a proton perpendicular temperature as high as 10^7 K in the inner corona can accelerate a fast solar wind, as is also shown in the other studies [e.g., *Esser et al.*, 1997; *Olsen and Leer*, 1996, 1998]. The high perpendicular temperature in the inner corona is much higher than UVCS observations [*Kohl et al.*, 1998; *Cranmer et al.*, 1999] but comparable to the broad component of hydrogen velocity distribution in the inner corona given by *Kohl et al.* [1996]. At 5.8 R_S, the proton parallel temperature increases to 6×10^6 K and protons become isotropic. This significant parallel heating is the result of an energy transport between perpendicular and parallel degrees of freedom as explained in section 3.1 and by *Olsen and Leer* [1999]. Here the maximum value of the perpendicular heat flux $q_{p\perp}$ is ~ 3 times as large as the value in model 1. In model 4, since no momentum addition is given to protons, the effect of the energy transport between perpendicular and parallel degrees of freedom is more remarkable. Without extended perpendicular heating and parallel cooling the proton temperature anisotropy $T_{p\|}/T_{p\perp}$ is as large as 270 at 1 AU. The extremely high parallel and low perpendicular temperature beyond $0.3R_S$ is contrary to in situ measurements, implying important physical processes are needed, namely, extended perpendicular heating and parallel cooling mechanisms.

The proton velocity distribution contours for model 4 are plotted in Figure 7 for comparison with the results by *Olsen and Leer* [1999]. These distribution contours are similar to those given by *Olsen and Leer* [1999]. As in Figures 3 and 5, the velocity distribution contours are Maxwellian at $1R_S$ but much less bi-Maxwellian at $1.4R_S$, implying that the collision-dominated region becomes smaller because of a stronger perpendicular heating in the inner corona. The strong heat flux in model 4 skews the velocity distribution contours much more strongly than in models 2 and 3. The negativity area in velocity space is much larger too. Since beyond $40R_S$ the proton perpendicular temperature is much smaller than the parallel temperature, the velocity distribution contours, which will be very narrow in the perpendicular direction, are not given.

Figure 7

3.4. Validity of the 16-Moment Approximation

In the 16-moment expansion of the distribution function in (1)–(3) the higher-order moments are responsible for the skewness of the velocity distribution. If the higher-order moments are very strong, the 16-moment bi-Maxwellian transport equations may not be hyperbolic and could lead to the unphysical result that the generated velocity distribution has negative values in some velocity space. When this happens, the 16-moment expansion is not applicable. It is found that this does not become a serious problem in our models: the smallest value of the normalized distribution f (the maximum value is 1) is only slightly less than 0. For example, in Figures 3 and 5 the smallest value of the normalized proton distribution is ~ -0.01. One can also test this by comparing values of electron and proton parallel and perpendicular heat flux densities obtained from the models with the corresponding thermalized heat flows, defined for a given species by [*Demars and Schunk*, 1991]

$$
\begin{aligned}
(q)_{th} &= nmv_{th}^3/2 \ , \\
(q_\parallel)_{th} &= nmv_{\parallel th}^2 v_{th} \ , \\
(q_\perp)_{th} &= nmv_{\perp th}^2 v_{th}/2 \ ,
\end{aligned}
\tag{24}
$$

where the thermal velocities are defined as

$$
v_{th}^2 = 2\frac{k_B T}{m} \ , \ v_{\parallel th}^2 = \frac{2k_B T_\parallel}{m} \ , \ v_{\perp th}^2 = \frac{2k_B T_\perp}{m}. \tag{25}
$$

Here we adopt the hyperbolicity conditions for a bi-Maxwellian model given by *Palmadesso et al.* [1988], *Gombosi and Rasmussen* [1991], *Cordier* [1994a, b], and *Cordier and Girard* [1996]. The heat flux of parallel energy has to be compared with the free streaming heat flux defined as $(q_\parallel)_f = nm(k_B T_\parallel/m)^{3/2}$, and the heat flux of perpendicular energy has to be compared with the free streaming of perpendicular energy defined as $(q_\perp)_f = nk_B T_\perp (k_B T_\parallel/m)^{1/2}$. This hyperbolicity condition can be written as

$$
q_e < (q_e)_f = (q_e)_{th} \ , \ q_{p\parallel} < 0.91 (q_{p\parallel})_f \ , \ q_{p\perp} < (q_{p\perp})_f . \tag{26}
$$

Figure 8

The ratios $q_e/(q_e)_f$, $q_{p\parallel}/(q_{p\parallel})_f$, and $q_{p\perp}/(q_{p\perp})_f$ are shown in Figure 8 with values from model 3 as solid, dotted, and dashed lines, respectively. These ratios are always < 1, indicating that the 16-moment description for protons is valid everywhere in the range of the distances considered. The eight-moment description for electrons is also valid.

4. Conclusions

This study demonstrates that 16-moment transport equations based on a bi-Maxwellian velocity distribution are a powerful tool to model the fast solar wind. The proton heat flux density in the 16-moment models is at least 2 orders of magnitude smaller than the classical Coulomb collision-dominated proton heat flux density. Only at the coronal base is the proton heat flux density close to its classical value. The electron heat flux density, on the other hand, is only slightly different from its classical value.

The model computations show that a high proton perpendicular temperature in the inner corona, as inferred from UVCS observations, implies a high proton perpendicular heat flux density there. The high proton perpendicular heat flux density can transport thermal energy to the parallel degree of freedom because of the expansion of the flow. While the perpendicular temperature is fairly close to the observed values, the models yield a proton parallel temperature that is much higher than the values observed in interplanetary space when additional parallel cooling is not adopted. These results confirm the conclusion reached earlier by *Hu et al.* [1997] that a parallel cooling mechanism is needed in high-speed streams beyond $\sim 50\ R_S$ if that temperature component is high in the inner corona. Note that *Hu et al.* [1997] used a simple approximation for the proton heat flux density. Hence the 16-moment description of proton transport equations lends even stronger support for the idea that a parallel cooling mechanism is needed for protons.

The 16-moment bi-Maxwellian solar wind model shows a clear transition from the collision-dominated region at the coronal base to the collison-free region in the interplanetary space. The proton velocity distribution functions are Maxwellian at the coronal base but become strongly skewed in the inner corona where the proton perpendicular temperature and perpendicular heat flow are large. Despite the fact that the 16-moment bi-Maxwellian description can model the heat flux in the fast solar wind it fails to reproduce the in situ measured velocity distributions. To generate the observed proton velocity distributions, some nonthermal processes may be necessary. These nonthermal processes may play a role similar to Coulomb collisions to isotropize the protons. To show the merit of the 16-moment models, ad hoc heating and momentum functions were used to heat and accelerate the solar wind. To understand better the physical mechanism of the solar wind heating and acceleration, it is essential to apply different solar wind heating mechanisms to the 16-moment models and study their capability to generate a realistic solar wind. It is also possible that these heating mechanisms can produce quite different temperature gradients and heat flux levels. The resulting skewness from the heat flux will be different too. Recently, *Li et al.* [1999] proposed that turbulence-driven ion cyclotron waves can heat protons in the perpendicular direction as well as cool them in the parallel direction. The 16-moment models presented here reinforce the likelihood that the solar wind is heated by ion cyclotron waves. However, how the ion cyclotron waves regulate the velocity distribution is not known and is desperately needed.

Worth noting is that a bi-Maxwellian velocity distribution function-based approximation is only one choice. It was also suggested that proton velocity distribution functions in astrophysical winds can be approximated by a polynomial expansion based on an exact solution of the BGK equation [*Bhatnagar et al.*, 1954] for moderately ionized plasmas [*Leblanc* *and Hubert*, 1997, 1998]. The corresponding transport equations have been given by *Leblanc and Hubert* [1998]. Leblanc and Hubert have chosen zero-order distribution functions mainly to take better into account the role of the superthermal part of the distribution function in the resolution of the Fokker Planck equation by a multimoment approach. Their approximation has another advantage that the approximation can avoid the negative value in the bi-Maxwellian approximation. It will be very interesting to apply these models to the solar wind.

Acknowledgments. I would like to thank S. R. Habbal for helpful discussions and input. This work is supported by NASA grant NAG5-6271.

Janet G. Luhmann thanks Oystein Lie-Svendsen and Francois Leblanc for their assistance in evaluating this paper.

References

Barakat, A.R., and R.W. Schunk, Transport equations for multicomponent anisotropic space plasma: A review, *Plasma Phys., 24*, 389, 1982.

Blelly, P.L., and R.W. Schunk, A comparative study of the time-dependent standard 8-, 13- and 16-moment transport formulations of the polar wind, *Ann. Geophys., 11*, 443, 1993.

Bhatnagar, P.L., E.P. Gross, and M. Krook, A model for collision processes in gases, *Phys. Rev., 94*, 511, 1954.

Braginskii, S. I., Transport processes in a plasma, in *Reviews of Plasma Physics*, vol. 1, p. 205, Consult. Bur., New York, 1965.

Burgers, J. M., Flow equations for composite gases, Academic, San Diego, Calif., 1969.

Cordier, S., Hyperbolicity of Grad's extension of hydrodynamic models arising from ionospheric plasma modeling, 1, The single species case, *Math. Method Models Appl. Sci., 4*, 625, 1994a.

Cordier, S., Hyperbolicity of Grad's extension of hydrodynamic models arising from ionospheric plasma modeling, 2, The two-species case, *Math. Method Models Appl. Sci., 4*, 647, 1994b.

Cordier, S., and L. Girard, Hyperbolicity analysis of multimoment plasma models: Application to auroral plasma outflows along magnetic field lines, *Planet. Space Sci., 44*, 225, 1996.

Cranmer, S. R., et al., An empirical model of a polar coronal hole at solar minimum, *Astrophys. J., 511*, 481, 1999.

David, C., A. H. Gabriel, G. Bely-Dubau, A. Fludra, P. Lemaire, and K. Wilhelm, Measurement of the electron temperature gradient in a solar coronal hole, *Astron. Astrophys., 336*, L90, 1998.

Demars, H. G., and R. W. Schunk, Transport equations for multispecies plasmas based on individual bi-Maxwellian distributions, *J. Phys. D Appl. Phys., 12*, 1051, 1979

Demars, H. G., and R. W. Schunk, Solar wind proton velocity distributions: Comparison of the bi-Maxwellian based 16-moment expansion with observations, *Planet. Space Sci., 38*, 1091, 1990.

Demars, H. G., and R. W. Schunk, Solutions to bi-Maxwellian transport equations for radial solar wind beyond 28 R_S, *Planet. Space Sci. 39*, 435, 1991.

Demars, H. G., and R. W. Schunk, A multi-ion generalized transport model of the polar wind, *J. Geophys. Res., 99*, 2215, 1994.

Dulk, G. A., K. V. Sheridan, S. F. Smerd, and G. L. Withbroe, Radio and EUV observations of a coronal hole, *Solar Phys., 52*, 349, 1977.

Esser, R., S. R. Habbal, W. A. Coles, and J. V. Hollweg, Hot protons in the inner corona and their effects on the flow properties of the solar wind, *J. Geophys. Res., 102,* 7063, 1997.

Fisher, R. R. and M. Guhathakurta, Physical properties of the polar coronal rays and holes as observed with SPARTAN 201-01 coronagraph, *Astrophys. J., 447*, L139, 1995.

Ganguli, S. B., and P. J. Palmadesso, Plasma transport in the auroral return current region, *J. Geophys. Res., 92*, 8673, 1987.

Ganguli, S. B., H. G. Mitchell Jr., P. J. Palmadesso, Behavior of ionized plasma in the high latitude topside ionosphere: The polar wind, *Planet. Space Sci., 35*, 703, 1987.

Goldstein, B. E., et al., Ulysses plasma parameters: Latitudinal, radial, and temporal variations, *Astron. Astrophys., 316*, 296, 1996.

Gombosi, T. I., and A. F. Nagy, Time-dependent polar wind modeling, *Adv. Space Res., 8(5)*, 59, 1988.

Gombosi, T. I., and C. E. Rasmussen, Transport of gyration-dominated space plasmas of thermal origin, 1, Generalized transport equations, *J. Geophys. Res., 96*, 7759, 1991.

Gross, E. P., and M. Krook, Model for collision processes in gases, *Phys. Rev., 102*, 593, 1956.

Hollweg, J. V., Viscosity and the Chew-Goldberger-Low equations in the solar corona, *Astrophys. J., 306*, 730, 1986.

Hu, Y. Q., R. Esser, and S. R. Habbal, A fast solar wind model with anisotropic proton temperature, *J. Geophys. Res., 102,* 14,661, 1997.

Kohl, J. L., L. Strachan, and L. D. Gardner, Measurement of hydrogen velocity distributions in the extended solar corona, *Astrophys. J., 465,* L141, 1996.

Kohl, J.L., et al., UVCS/SOHO empirical determinations of anisotropic velocity distributions in the solar corona, *Astrophys. J., 501,* L127, 1998.

Kopp, R. A. and T. E. Holzer, Dynamics of coronal hole regions, 1, Steady polytropic flow with multiple critical points, *Solar Phys., 49*, 43, 1976.

Krook, M., Dynamics of rarefied gases, *Phys. Rev., 99*, 1896, 1955.

Leblanc, F., and D. Hubert, A generalized model for the proton expansion in astrophysical winds, I, The velocity distribution function representation, *Astrophys. J., 483*, 464, 1997.

Leblanc, F., and D. Hubert, A generalized model for the proton expansion in astrophysical winds, II, The associated set of transport equations, *Astrophys. J., 501*, 375, 1998.

Leer, E., and W. I. Axford, A two-fluid solar wind model with anisotropic proton temperature, *Solar Phys., 23,* 238, 1972.

Li, X., A 16-moment fast solar wind model, *Space Sci. Rev.*, in press, 1999.

Li, X., S. R. Habbal, J. V. Hollweg, and R. Esser, Heating and cooling of protons by turbulence-driven ion cyclotron waves in the fast solar wind, *J. Geophys. Res., 104,* 2521, 1999.

Livi, E., and E. Marsch, Comparison of the Bhatnagar-Gross-Krook approximation with the exact Coulomb collision operator, *Phys. Rev. A, 34*, 533, 1986.

Marsch, E., K. H. Muhlhauser, R. Schwenn, H. Rosenbauer, W. Pilipp, and F. M. Neubauer, Solar wind protons: Three dimensional velocity distributions and derived plasma parameters measured between 0.3 AU and 1 AU, *J. Geophys. Res., 87,* 52, 1982.

Marsch, E., and A. K. Richter, Helios observational constraints on solar wind expansion, *J. Geophys. Res., 89,* 6599, 1984

Marsch, E., W. G. Philip, K. M. Thieme, and H. Rosenbauer, Cooling of solar wind electrons inside 0.3 AU, *J. Geophys. Res., 94*, 6893, 1989.

Marsch, E., Kinetic physics of the solar wind plasma, in *Physics of the Inner Heliosphere*, edited by R. Schwenn and E. Marsch, p. 45, Spring-Verlag, New York, 1991.

McKenzie, J. F., M. Banaszkiewicz, and W. I. Axford, The fast solar wind, *Geophys. Res. Lett., 24*, 2877, 1997.

Olsen, E. L., and E. Leer, An eight-moment approximation two-fluid model of the solar wind, *J. Geophys. Res., 101,* 15,591, 1996.

Olsen, E. L., E. Leer, and O. Lie-Svendsen, An eight-moment model parameter study of the solar wind: Dependence on variations in coronal heating, *Astron. Astrophys., 338*, 747, 1998.

Olsen, E. L., and E. Leer, A study of solar wind acceleration based on gyro-tropic transport equations, *J. Geophys. Res., 104,* 9963, 1999.

Oraevskii, V., R. Chodura, and W. Feneberg, Hydrodynamic equations for plasmas in strong magnetic field, I, *Plasma Phys., 10*, 819, 1968.

Palmadesso, P. J., S. B. Ganguli, and H. G. Mitchell, Multi-moment fluid simulations of transport processes in the auroral zones, in *Modeling Magnetospheric Plasma, Geophys. Monogr. Ser.*, vol. 44, edited by T.E. Moore and J.H. Waite, p. 133, AGU, Washington D.C., 1988.

Rosner, R., W. H. Tucker, and G. S. Vaiana, Dynamics of the quiescent solar corona, *Astrophys. J., 220*, 643, 1978.

Sandbæk, Ø., and E. Leer, Acceleration and heating of two-fluid solar wind by Alfvén waves, *Astrophys. J., 423,* 500, 1994.

Schunk, R. W., and D. S. Watkins, Comparison of solutions to the thirteen-moment and standard transport equations for low speed thermal proton flows, *Planet. Space Sci., 27*, 433, 1979.

Spitzer, L., Jr., and R. Härm, Transport phenomena in a completely ionized gas, *Phys. Rev., 89*, 977, 1953.

Wilhelm, K., E. Marsch, B. N. Dwivedi, D. M. Hassler, P. Lemaire, A. H. Gabriel, and M. C. E. Huber, The solar corona above polar coronal holes as seen by *SUMER* on *SOHO*, *Astrophys. J., 500*, 1023, 1998.

Withbroe, G. L., Models for the solar transition layer, paper presented at OSO-8 Workshop, Lab. for Atmos. and Space Phys., Univ. of Colo., Boulder, 1977.

Withbroe, G.L., The temperature structure, mass, and energy flow in the corona and inner solar wind, *Astrophys. J., 325,* 442, 1988.

X. Li, Harvard-Smithsonian Center for Astrophysics, 60 Garden Street, Cambridge, MA 02138. (email: xli@cfa.harvard.edu.)

Received February 26, 1999; revised May 6, 1999; accepted June 7, 1999.

This preprint was prepared with AGU's LATEX macros v5.01. File revise formatted July 27, 1999.

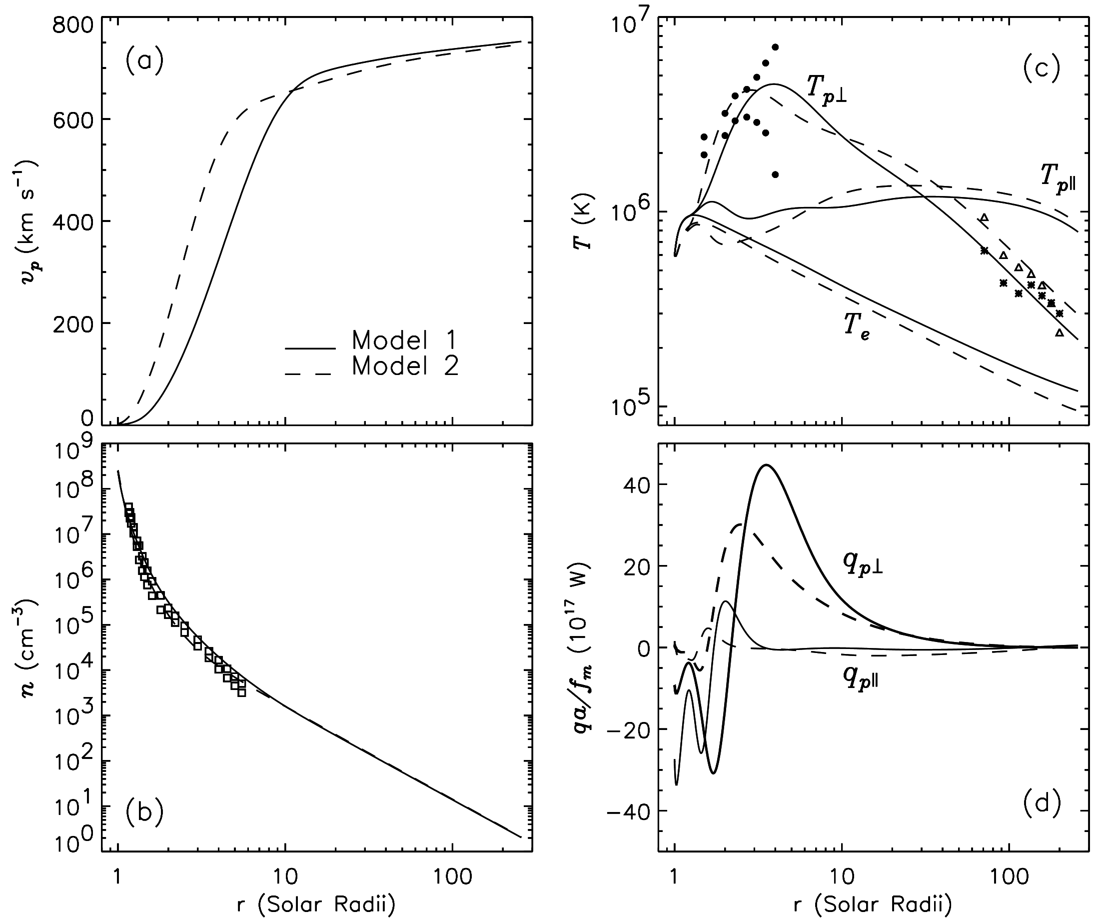

Figure 1. Two fast solar wind models with different flow tube geometries; model 1, radial geometry given by the solid lines and model 2 (f_m =6) given by the dashed lines. (a) velocity, (b) electron density (the open boxes represent the observed upper and lower electron density limits given by *Fisher and Guhathakurta* [1995]), (c) proton and electron temperatures (the solid circles represent the observed upper and lower perpendicular temperatures of neutral hydrogen derived from the line width measurements of hydrogen Lyα in coronal holes [*Kohl et al.*, 1998], and the triangles and stars represent the perpendicular and parallel proton temperatures observed by *Helios* [*Marsch et al.*, 1982]), (d) proton parallel and perpendicular heat flux densities multiplied by a/f_m.

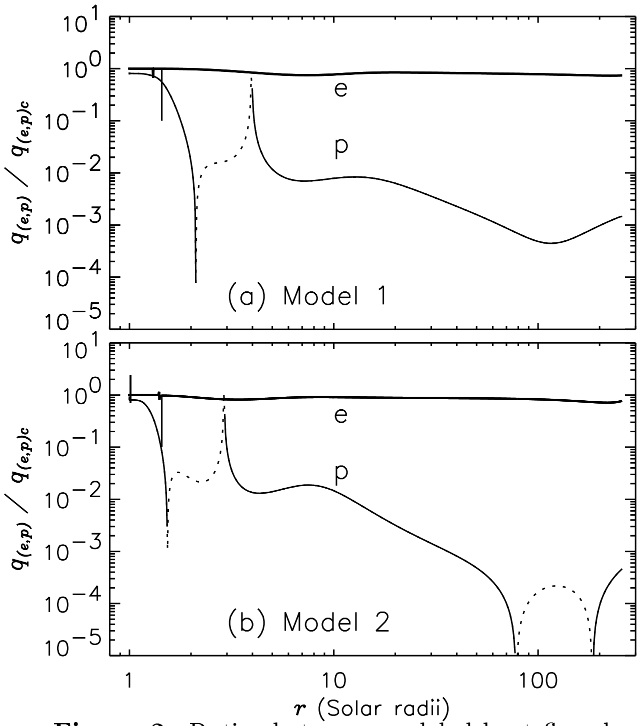

Figure 2. Ratios between modeled heat flux densities and corresponding classical values of (a) model 1 and (b) model 2. The solid and dotted lines correspond to positive and negative values, respectively.

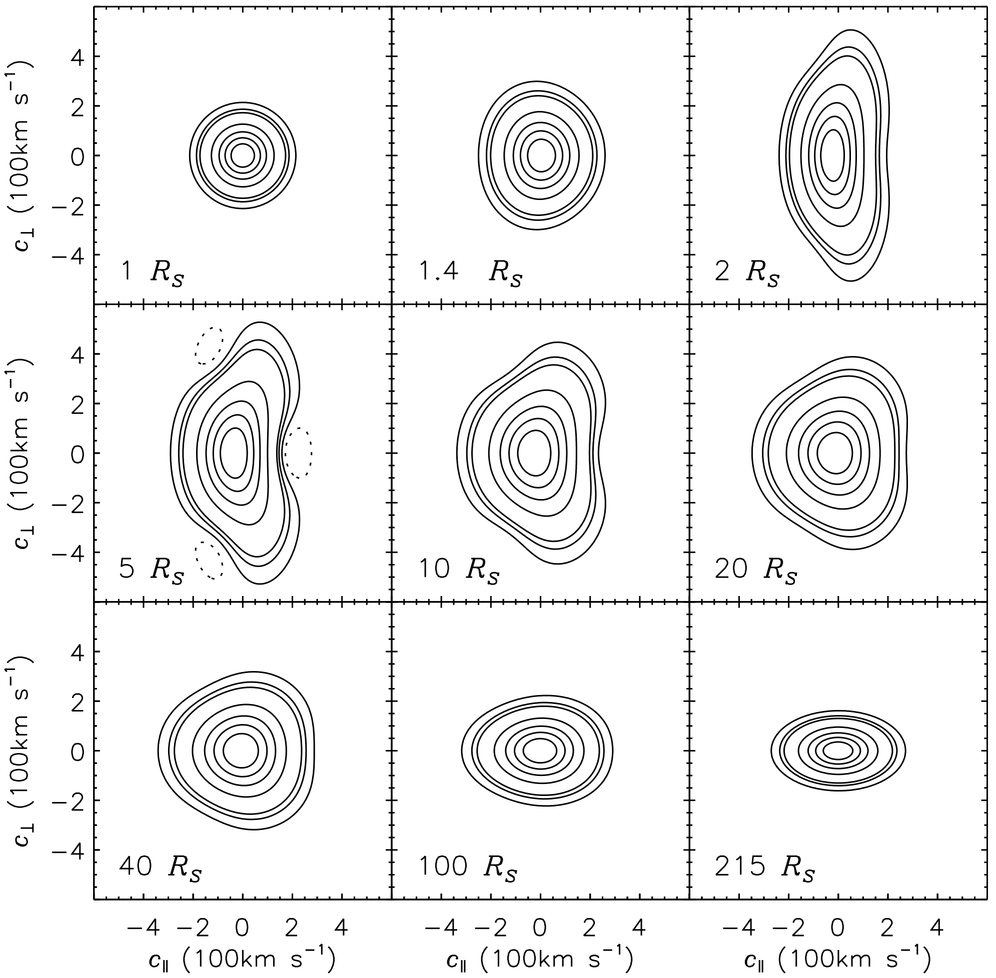

Figure 3. Two-dimensional proton velocity distribution contours of model 2 in the plane defined by the magnetic field vector and an arbitrary direction vector in velocity space ($c_\parallel$ is shifted to the solar wind corotating frame). The distribution function f has been normalized so that its maximum value is 1. The innermost to the outermost solid contours correspond to fractions 0.01, 0.03, 0.05, 0.2, 0.4, 0.6, and 0.8 of the normalized distribution function. The dotted contours correspond to a negative value of −0.005. The positive direction of $c_\parallel$ represents the direction away from the Sun along the interplanetary spiral magnetic field.

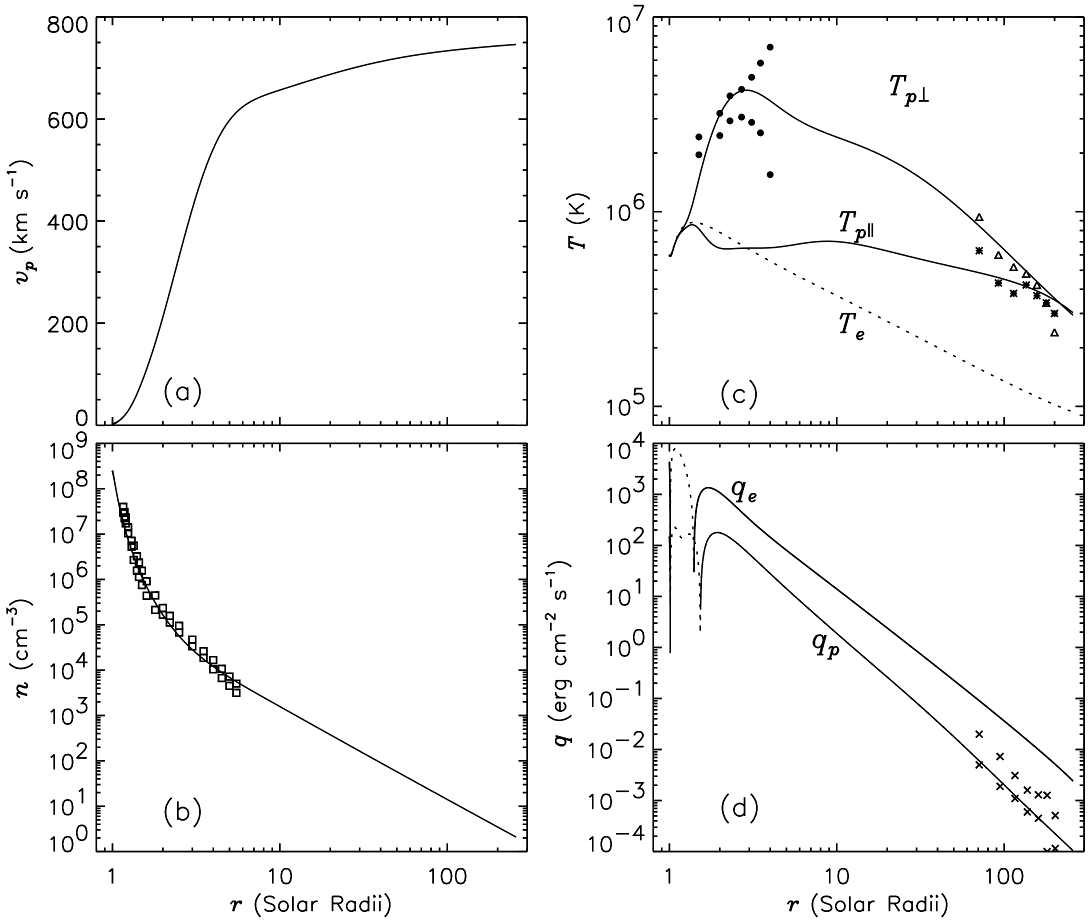

Figure 4. Model 3: same as Figure 1 except Figure 4d. The crosses represent the total ion heat flux in the fast solar wind [*Marsch and Richter*, 1984]. In model 3 an ad hoc cooling effect is applied to protons in the equation for $T_{p\|}$.

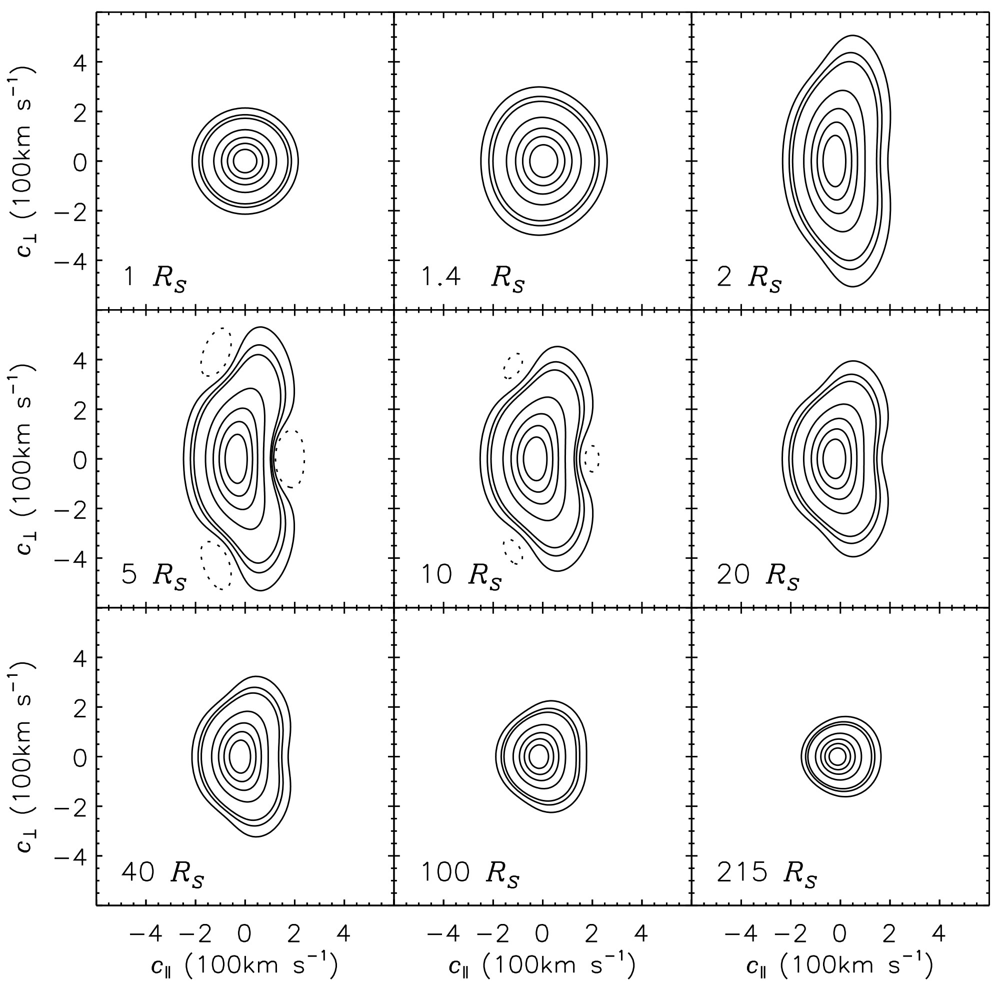

Figure 5. Same as Figure 3 but for model 3.

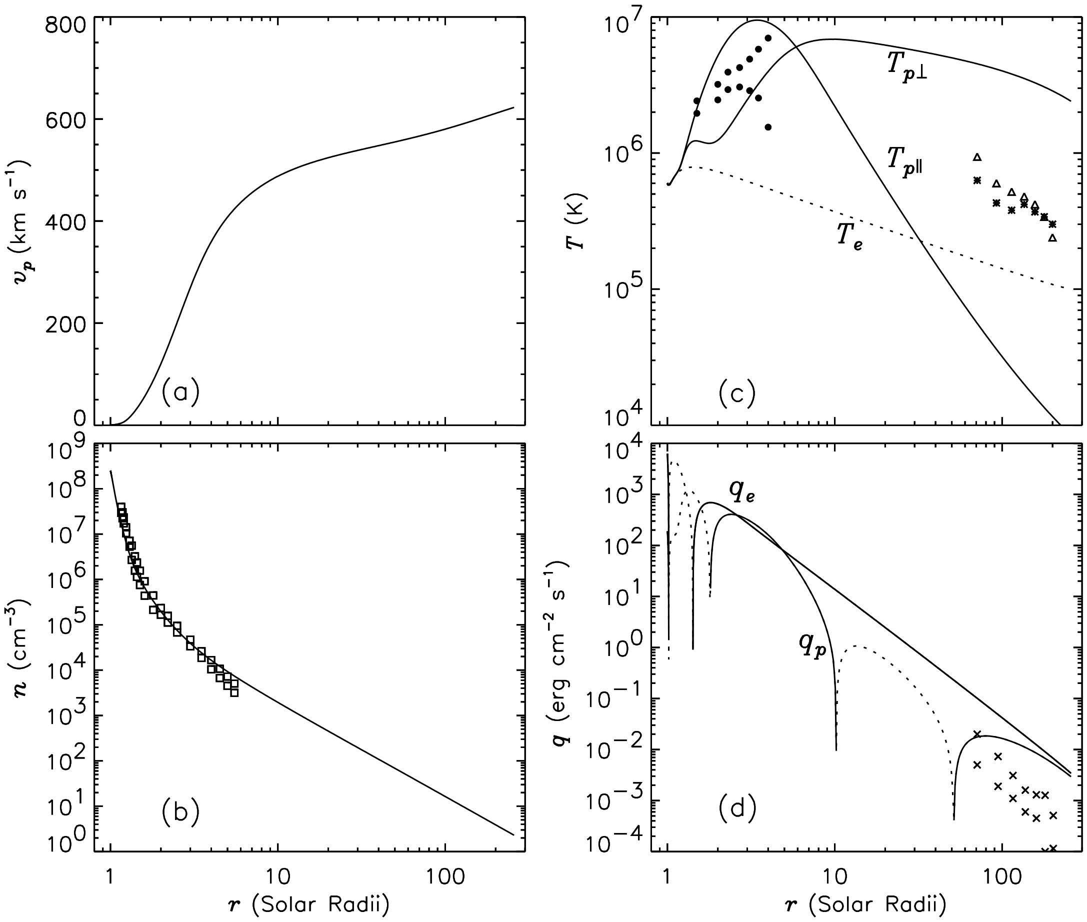

Figure 6. Same as Figure 1 but for model 4. In model 4, extended heating and momentum addition have been dropped: $Q_{p2} = Q_{p3} = D_0 = 0$.

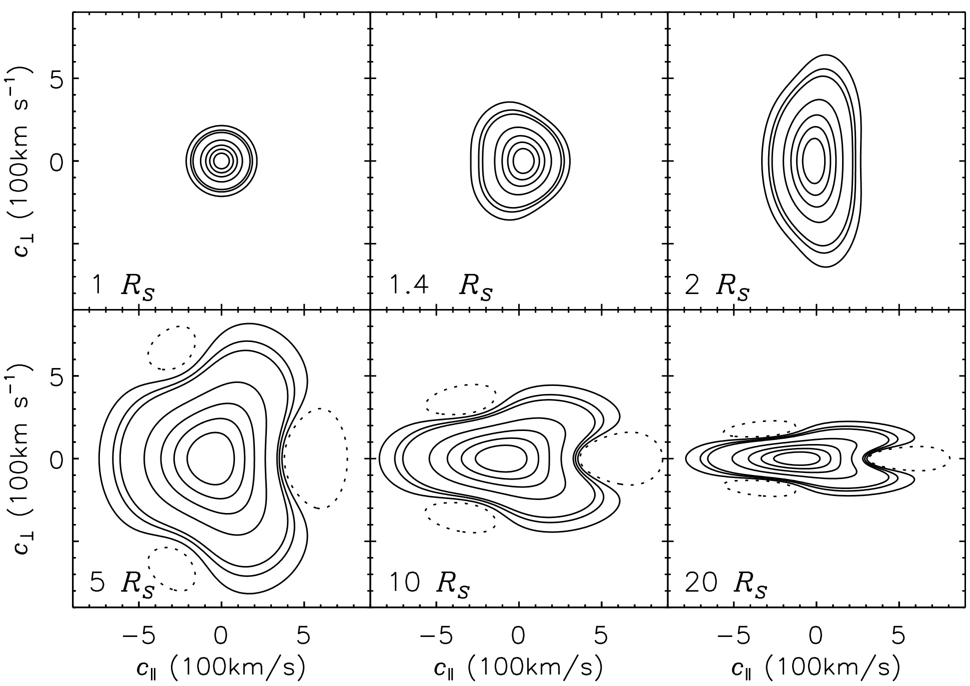

Figure 7. Same as Figure 3 but for model 4.

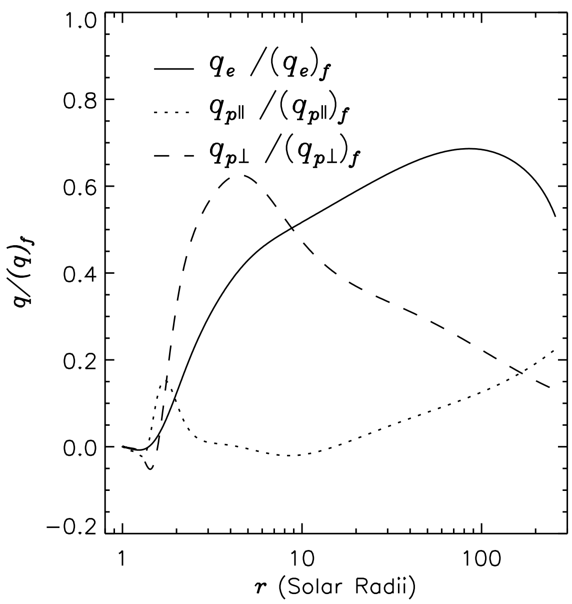

Figure 8. Ratios between electron and proton parallel and perpendicular heat flux densities obtained from model 3 and corresponding thermalized heat flow. Solid, dotted, and dashed lines correspond to $q_e/(q_e)_f$, $q_{p\|}/(q_{p\|})_f$, and $q_{p\perp}/(q_{p\perp})_f$, respectively.